Biophysical Journal, Volume *118*

Supplemental Information

Dynamical Organization of Compositionally Distinct Inner and Outer Membrane Lipids of Mycobacteria

Pranav Adhyapak, Aswin T. Srivatsav, Manjari Mishra, Abhishek Singh, Rishikesh Narayan, and Shobhna Kapoor

SI Methods

Laurdan GP spectroscopy: Being a solvation sensitive probe, Laurdan is employed to determine the hydration and order of membranes. The emission spectra of Laurdan exhibit spectral shifts due to dielectric relaxation and can be analysed by calculating the generalised polarisation using Eq. S1.

$$GP = \frac{I_{440} - I_{490}}{I_{440} + I_{490}} \quad \text{(S1)}$$

Where, I_{440} and I_{490} refer to the intensities at 440 nm and 490 nm characteristic for ordered (gel) phase and fluid, liquid crystalline phase respectively.

Membrane fluidity studies: Fluorescence anisotropy measurements were done using Laurdan, TMA-DPH and DPH using a Varian Cary Eclipse spectrofluorometer attached with a polarizer (varian manual Polarizer Accessory). Fluorescence intensity was measured with excitation and emission polarizer parallel to each other (both at 0^o, I_0) and repeated with polarizer perpendicular (excitation: 0^o, emission: 90 ^{o}, I_{90}). The degree of fluorescence steady-state anisotropy (r) was calculated from Eq. S2.

$$r = \frac{I_{ii} - (G * I_{\perp})}{I_{ii} + (2G * I_{\perp})} \quad \text{(S2)}$$

where, G is the correction factor obtained from ratio of emission intensity at 0 ^{o} and 90 ^{o} with the excitation polarizer oriented at 90 $^{o.}$

AFM Force Spectroscopy: Force spectroscopy was performed to gain insights into the resistance experienced by cantilever tip to rupture the bilayer. In this approach, force distance curves were recorded. The supported lipid bilayer is considered as a planar arrangement of adjacent lipid molecules. As the tip approach and indent the bilayer, the latter gets compressed, the molecular area underneath the tip changes and lipid positions fluctuate. Between the adjacent molecules of lipids, energy is elastically stored until the rupture point occurs. This creates a jump in force-distance curve, as the tip pierces through the bilayer. This jump is considered as breakthrough force event.

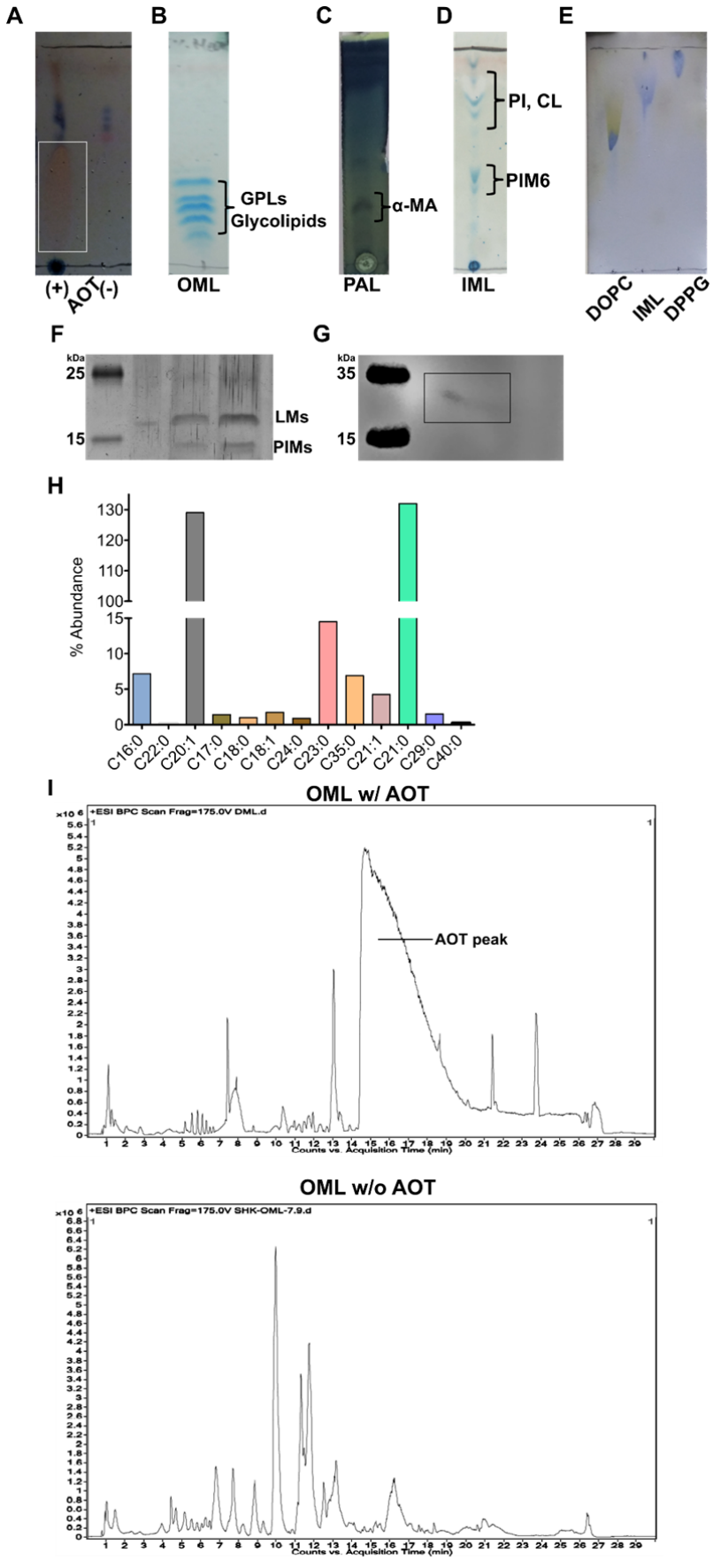
A
B
C
D
E
(+)
AOT
(-)
OML
GPLs
Glycolipids
PAL
α-MA
IML
PI, CL
PIM6
DOPC
IML
DPPG
F
kDa
25
15
LMs
PIMs
G
kDa
35
15
H
% Abundance
130
120
110
100
15
10
5
0
C16:0
C22:0
C20:1
C17:0
C18:0
C18:1
C24:0
C23:0
C35:0
C21:1
C21:0
C29:0
C40:0
I
OML w/ AOT
+ESI BPC Scan Frag=175.0V DML.d
AOT peak
Counts vs. Acquisition Time (min)
OML w/o AOT
+ESI BPC Scan Frag=175.0V SHK-OML-7.9.d
Counts vs. Acquisition Time (min)

Fig. S1 - (A-E) TLC profiles of extracted lipids. (A) TLC profile of OML with and without AOT developed in chloroform-methanol mixture (C:M) (9:1). The long ochre coloured spot confirmed the presence of AOT. (B) OML TLC developed in C:M (9.5:0.5). GPLs and glycolipids were visualized using anthrone spray. (C) Mycolic acid methyl esters developed in pet ether-diethyl ether (PE:DE) (85:15) and visualized using phosphomolybdic acid stain (PMA). (D) Glycolipids in IML were visualized using anthrone spray and developed in a mixture of chloroform–methanol–13M ammonia–1 M ammonium acetate–water (180:140:9:9:23). (E) Comparison of standard phospholipids with IML showed the mobility of IML being at an intermediate between DOPC and DPPG. (F) SDS PAGE profile of PIMs and LMs. (G) Western blot of LAM observed using anti-LAM antibody. (H) Fatty acid methyl esters of IML were subjected to GCMS to obtain information on the constituent fatty acids chains. (I) LCMS spectra showing the presence and absence of AOT before and after purification using column chromatography as described in Methods.

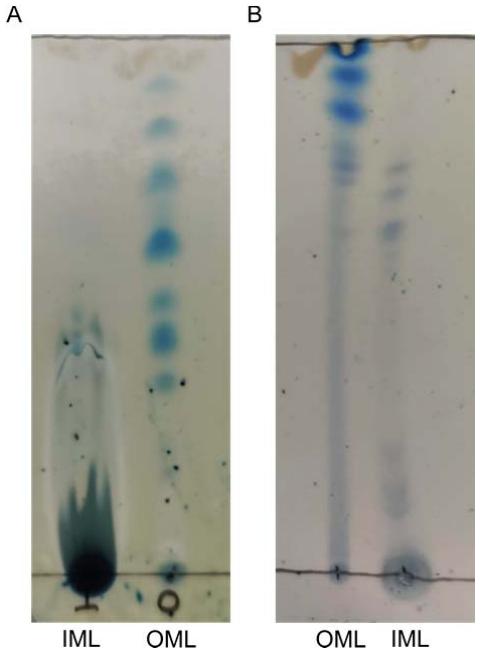

Figure S2 – Comparative TLC profiles of the lipids in OML and IML fractions detected using solvents of different polarity. A) in chloroform-methanol (9.7:0.3) and B) in chloroform–methanol–water (100:14:0.8). Both are visualized using anthrone spray.

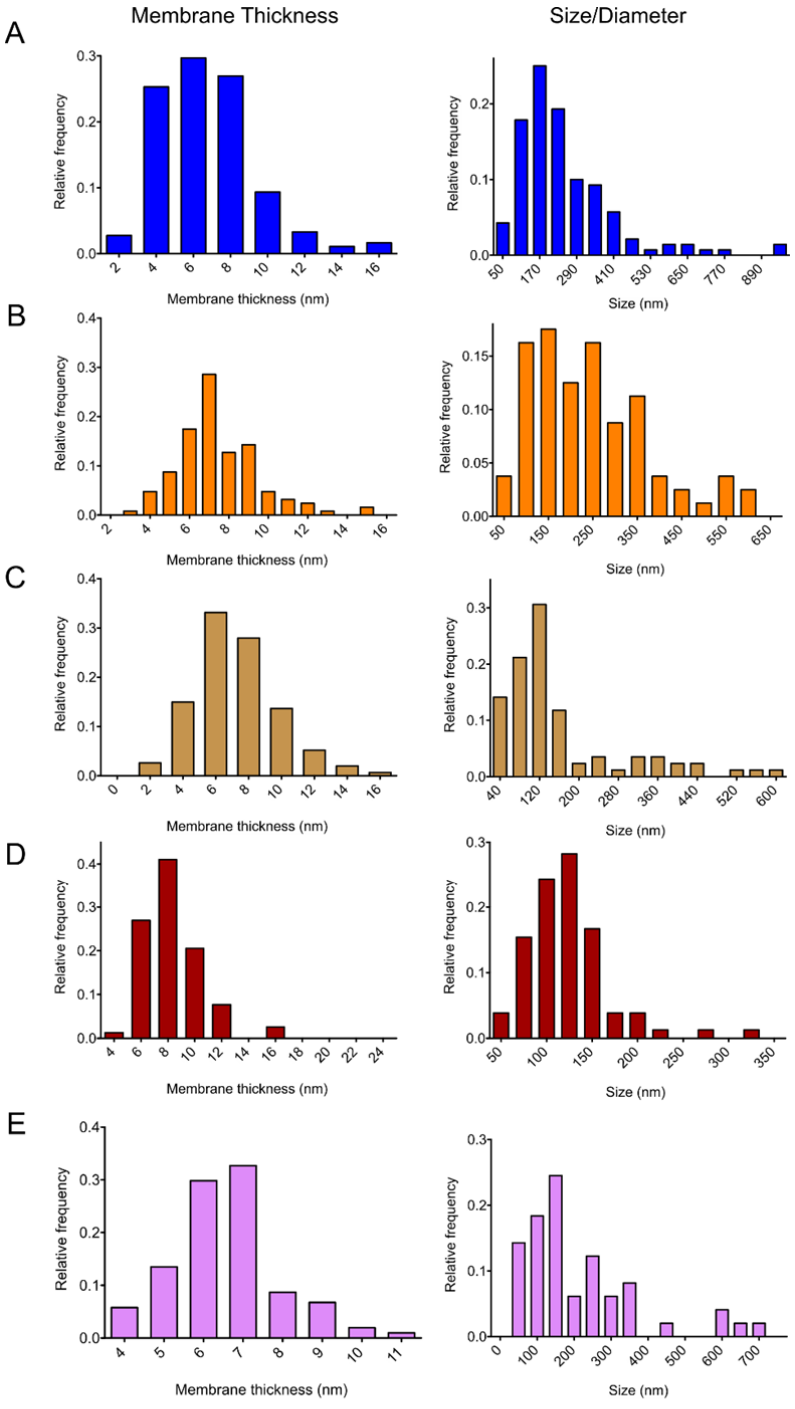

F

Lipid System	Mean zeta potential ± SD (mV)
IML	-24.71±0.60
OML	-16.82±0.31
OLP	-21.24±0.46
OL	-17.88±0.50
OP	-17.73±0.50

Fig. S3: Distribution of bilayer thickness and size of the mycobacterial lipid vesicles estimated from Cryo-TEM images. Bilayer thickness varies as (A) 6.7 ± 0.2 nm for IML (n=60), (B) 7.4 ± 0.2 nm for OML (n=42), (C) 7.3 ± 0.2 nm for OLP (n=50), (D) 8.3 ± 0.2 nm for OL (n=34), and (E) 6.6 ± 0.1 nm for OP (n=29) (mean ±SEM). Diameter/ size for IML, OML, OLP, OL and OP vesicles are 247.8 ± 13.3 nm (n=140), 241.8 ± 14.7 nm (n=80), 159.4 ± 13.4 nm (n=85), 123.4 ± 5.17 nm (n=78), 215.2 ± 23.2 nm (n=50) respectively (mean ± SEM).

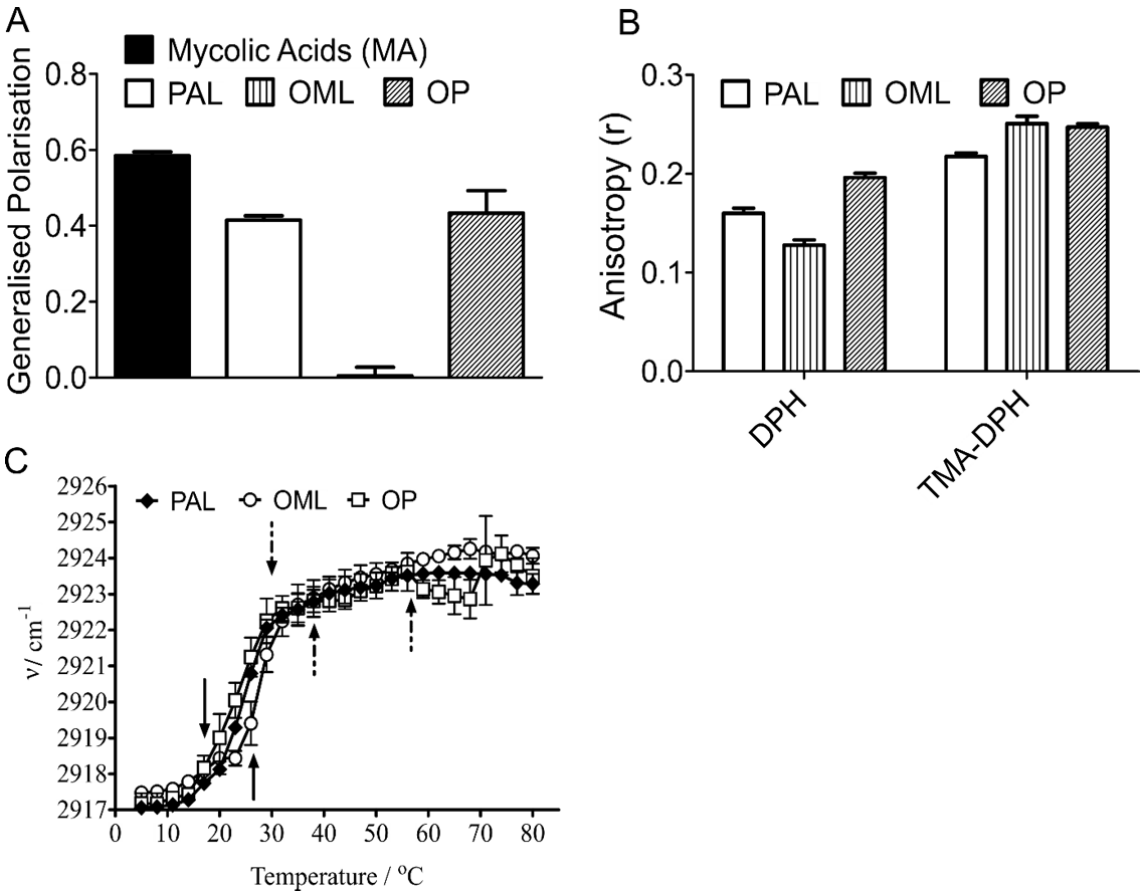

Fig. S4: PAL induced changes in membrane order and fluidity of mycobacterial outer membrane. (A) Laurdan GP (B) DPH and TMA-DPH anisotropy showing microviscosity changes in the deep hydrophobic acyl chain region and interfacial region respectively at 35 ºC in the indicated lipid systems. Data presented is mean (± SEM) of three independent experiments. (C) Acyl chain conformational dynamics of indicated lipid systems measured using FTIR monitoring $\nu_{asym}CH_2$. Black arrows indicate changes in slope, which can be, ascribed to onset of phase transitions. Solid arrows: main phase transition and dashed arrow indicate minor slope change and appearance of additional phases. Data presented is mean ± SD of three independent experiments.

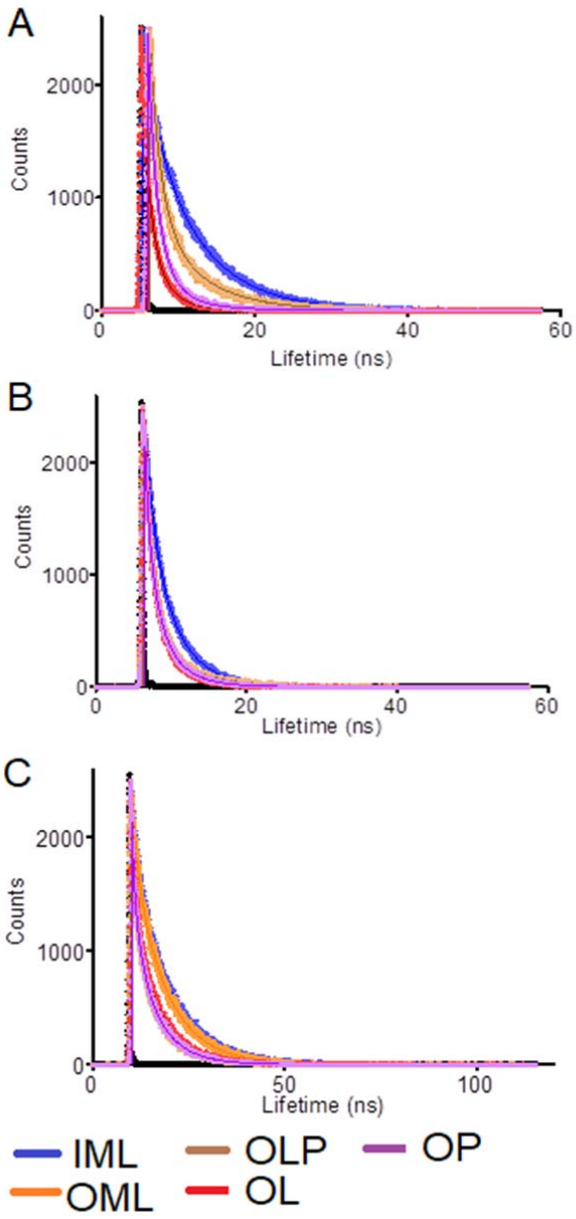

Fig. S5 – Representative Decay Curves of (A) Laurdan (B) TMA-DPH (C) DPH probes in various indicated mycobacterial model membrane lipid systems at RT.

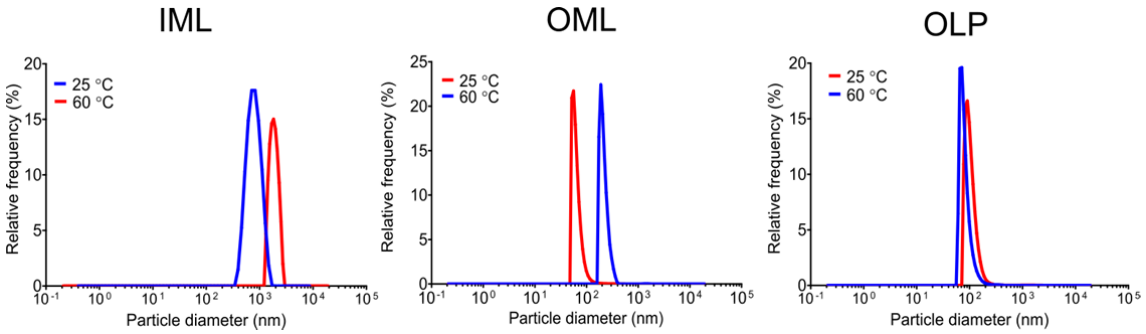

Fig. S6: **Temperature dependent size variation within** (A) IML (B) OML (C) OLP, suggesting intact integrity of vesicles at higher temperatures.

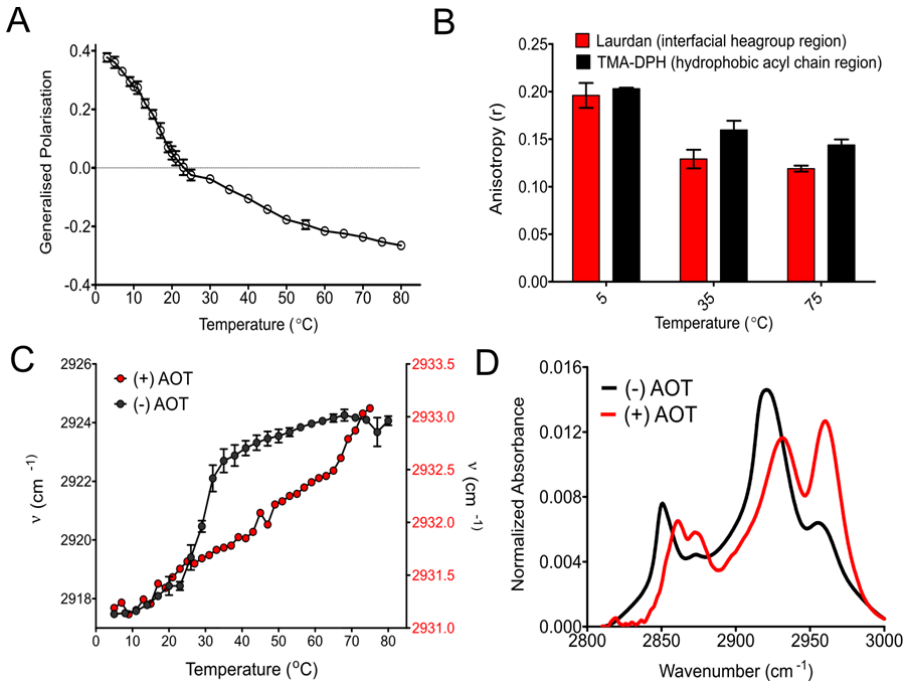

Fig. S7 – AOT alters the membrane properties of OML (A) Generalised polarisation curve showing that the presence of AOT reduces the apparent T_m of the OML system (compared to Fig. 3A). (B) Laurdan and TMA-DPH anisotropy of OML containing AOT. Data presented is mean (± SEM) of three independent experiments. (C) Internal vibrational mode of lipid acyl chains (asymmetric CH_2; $\nu_{asym}CH_2$) of OML and OML with AOT. Data is mean (± SD). Presence of AOT causes substantial disordering in the membrane bilayer indicated by higher wavenumbers. In addition, the phase transition is shifted to higher temperature suggesting significant effect on AOT on OM lipid phases (D) When AOT is present, the IR absorbance pattern has

characteristic doublet peaks at both 2920 and 2850 region. Data presented is mean (±SD).

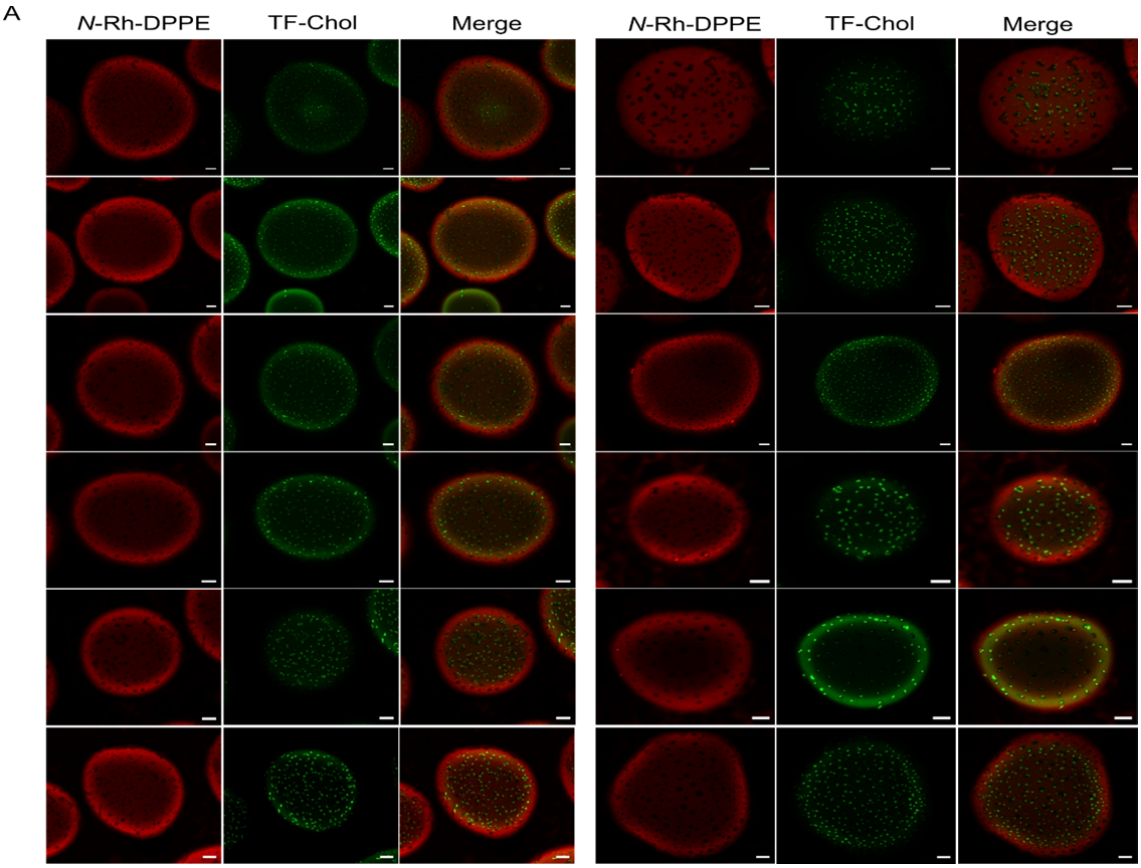

Fig. S8 – Representative confocal fluorescence microscopy images of IML GUVs. Fluorescence intensity was collected in two channels at 25 °C. *N-Rh*-DPPE was used as a marker labelling preferentially the l_d domains (detected by red channel), TopFluor-cholesterol partitions preferentially into l_o phase of the membrane. Scale bar: 20 μm.

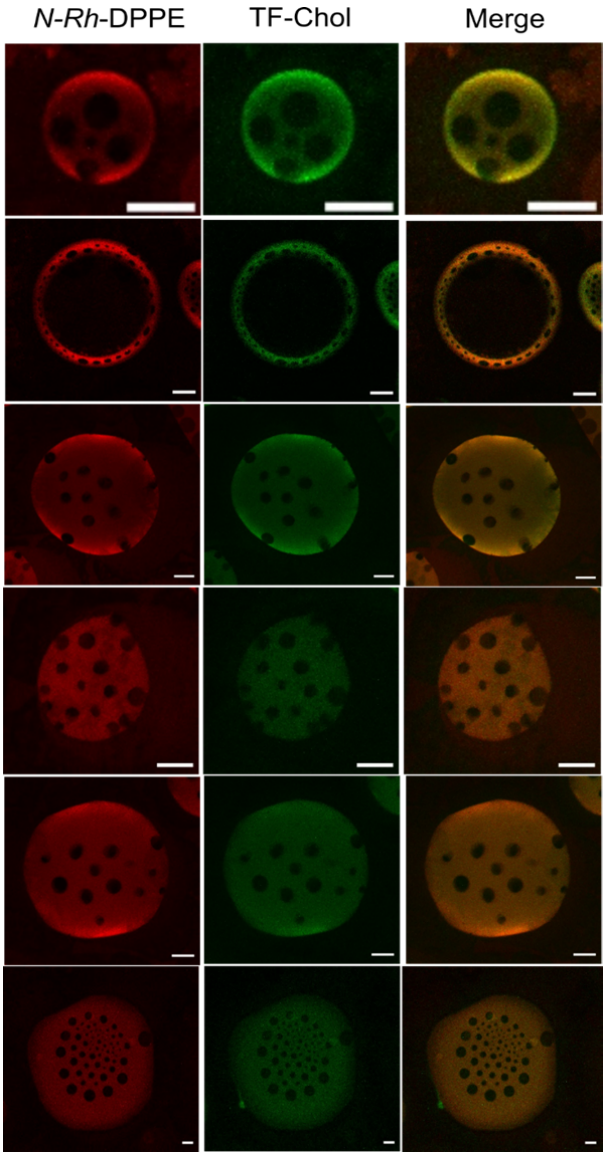

Fig. S9: Representative confocal fluorescence microscopy images of GUVs with solid-liquid phase separation. DOPC, DPPC, cholesterol were mixed (45:45:5 mol %) to form GUVs. Fluorescence intensity was collected in two channels at 25 °C. *N-Rh*-DPPE was used as a marker labelling preferentially the l_d domains (detected by red channel), TopFluor-cholesterol partitions preferentially into l_o phase of the membrane (green channel). Regions devoid of both the markers reflect the presence of gel phase domains. Scale bar: 20 μm.

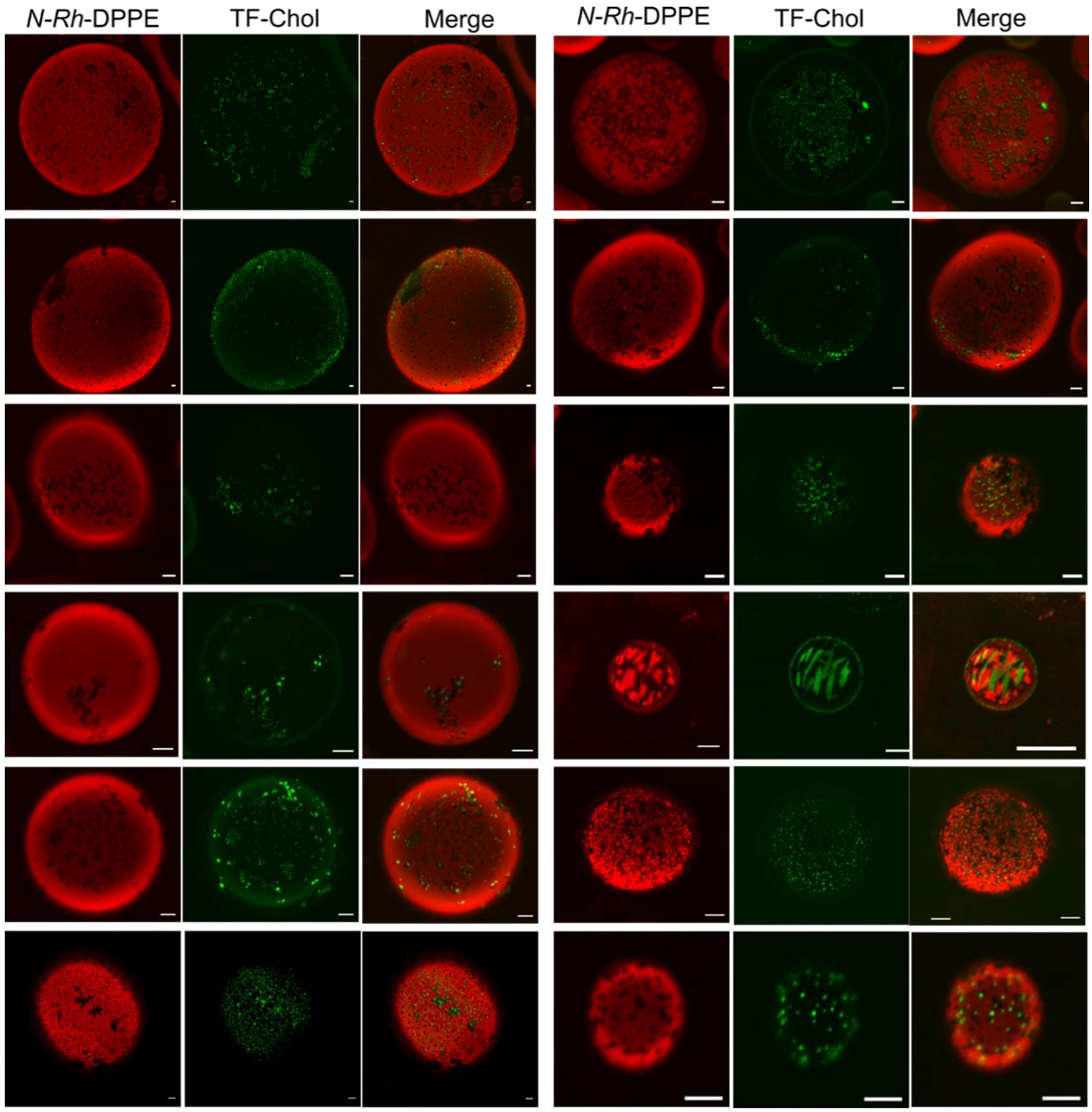

-

Fig. S10 – Representative confocal fluorescence microscopy images of OML GUVs. Fluorescence intensity was collected in two channels at 25 °C. *N-Rh*-DPPE was used as a marker labelling preferentially the l_d domains (detected by red channel), TopFluor-cholesterol partitions preferentially into l_o phase of the membrane. Scale bar: 20 μm.

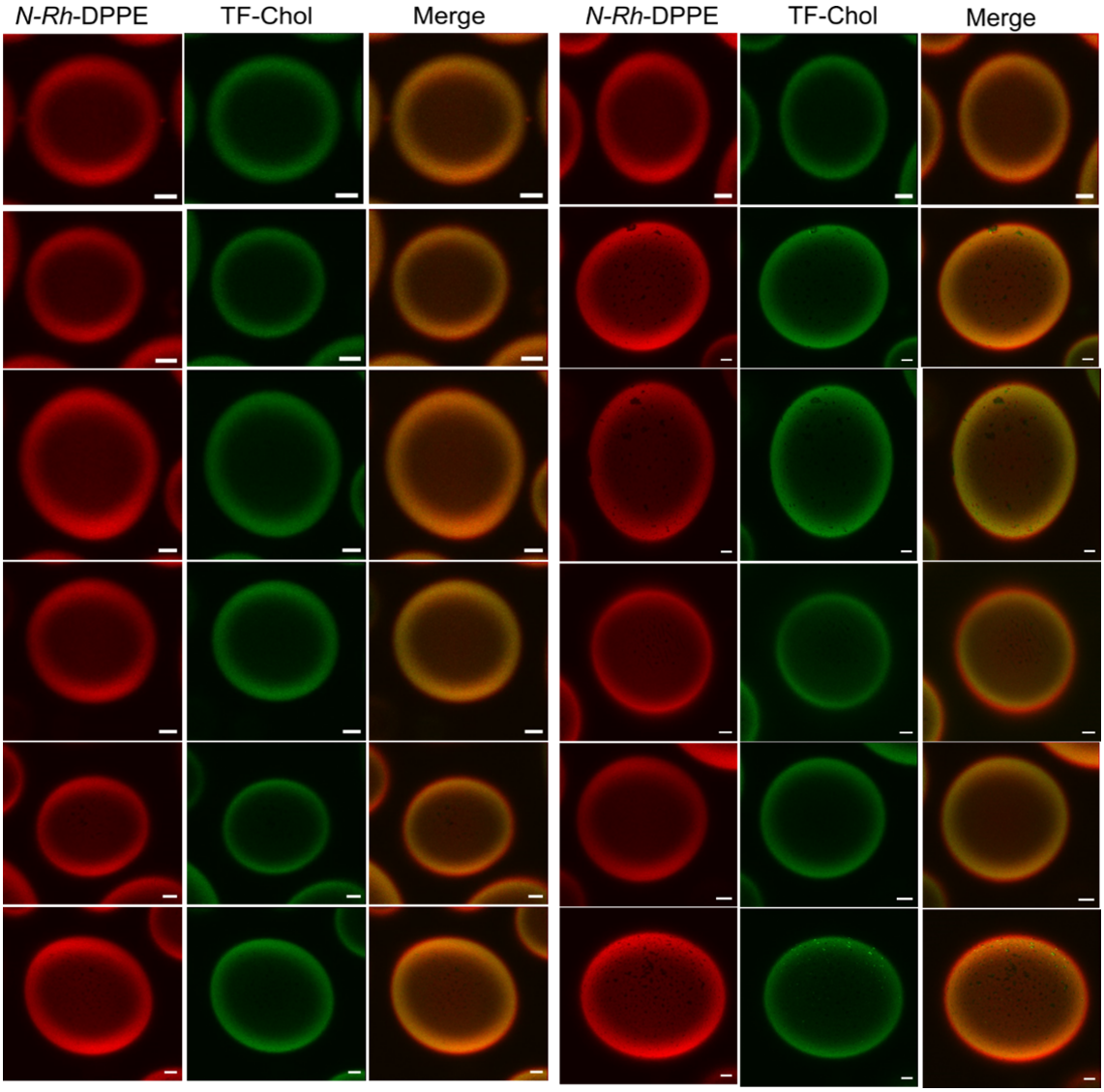

Fig. S11 – Representative confocal fluorescence microscopy images of OLP GUVs. Fluorescence intensity was collected in two channels at 25 °C. *N-Rh*-DPPE was used as a marker labelling preferentially the l_d domains (detected by red channel), TopFluor-cholesterol partitions preferentially into l_o phase of the membrane. Scale bar: 20 μm.

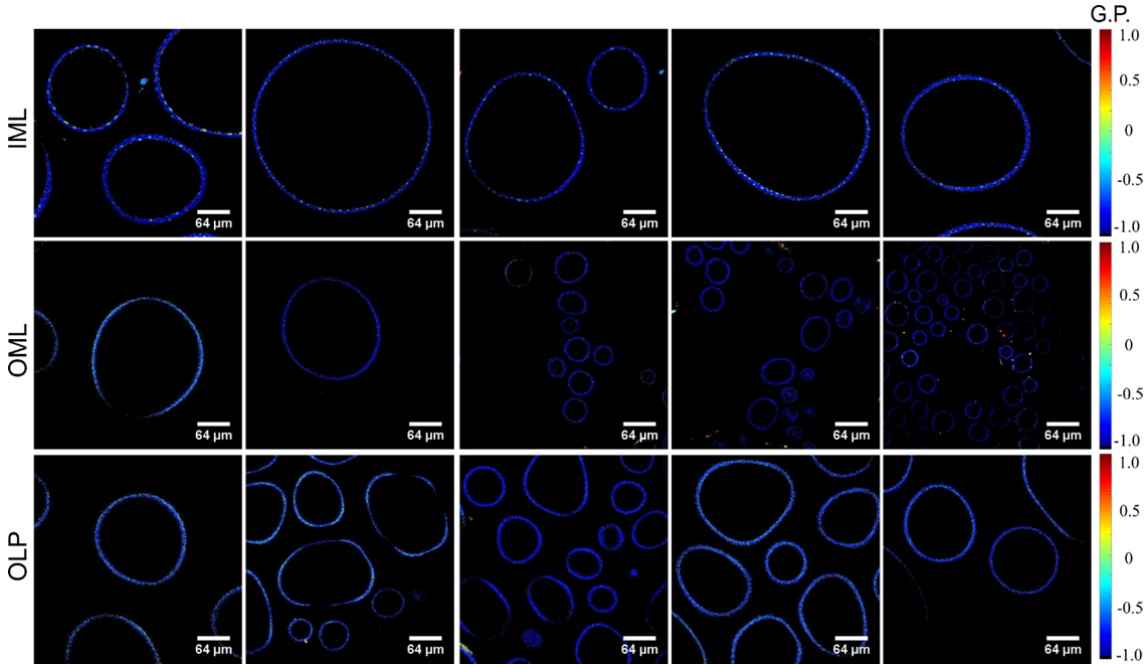

Fig. S12 – Laurdan GP images of mycobacterial model membrane revealing phase segregation and lipid microdomain formation. Pseudo-coloured Laurdan GP images of indicated GUVs at 25 °C. Scale Bar 64 µm.

Table S1: List of lipids identified through LCMS in OML and IML fractions after consulting the online mycobacterial databases. In bold are lipids characteristic of OM or IM fraction.

Sr No	Outer Membrane Lipids	Inner Membrane Lipids
1	**Ac2SGL** (C56)	**Ac1PIM1 (R1CO2H+R2CO2H+R3CO2H =55:3)**
2	**Alpha-MA (C89)**	**Ac1PIM1 (R1CO2H+R2CO2H+R3CO2H =55:5)**
3	Carboxylic exochelins threonine	**Ac1PIM2 (R1CO2H+R2CO2H+R3CO2H =51:3,R4=H)**
4	**DAT (C25:2)**	**Ac1PIM2 (R1CO2H+R2CO2H+R3CO2H =54:2,R4=H)**
5	**DAT (C26:0)**	**Ac1PIM2 (R1CO2H+R2CO2H+R3CO2H=49:0,R4=H)**
6	**DAT (C27:0)**	**Ac1PIM2 (R1CO2H+R2CO2H+R3CO2H=50:2,R4=H)**
7	**DAT (C32:0)**	**Ac1PIM3 (R1CO2H+R2CO2H+R3CO2H =50:0,R4=H)**
8	**DAT (C37:1)**	**Ac1PIM3 (R1CO2H+R2CO2H+R3CO2H=47:1,R4=H)**
9	**DAG (R1CO2H+R2CO2H=30:1)**	**Ac1PIM3 (R1CO2H+R2CO2H+R3CO2H=47:1,R4=H)**
10	**DAG (R1CO2H+R2CO2H=32:2)**	**Ac1PIM3 (R1CO2H+R2CO2H+R3CO2H=50:0,R4=H)**
11	Dideoxy Mycobactins (C18:1)	CM (Carboxymycobactins)
12	**Glycosylated phthiodiolone dimycocerosate (C106)**	DAG (C24:2)
13	**GPL-IIa/IV**	DAG (C25:0)
14	**GPL-IIb**	DDCM (dideoxycarboxymycobactin methyl esters) (C8:1)
15	**GPL-serovar 1**	DDCM (dideoxycarboxymycobactin methyl esters) (C12:1)
16	**Hydroxyphthioceranic acid (C34)**	DDCM (serine butyric acid dideoxycarboxymycobactins) (C9:1)
17	**Keto-MA (C83)**	DDCM (threonine/a-methyl serine ethylbutyric acid dideoxycarboxymycobactins) (C6:1)
18	Lysinated PG (C20:0)	L5P (lipopentapeptide)
19	Lyso PA (C20:4)	L5P (Lipopentides)
20	Lyso PE (C30:1)	LPA (C16:0)
21	Lyso PG (C14:0)	LPA (Lysophosphatidic Acid) (C20:4)
22	Lyso PG (C16:0)	LPE (C22:0)
23	Lyso phosphatidic acid (C29:1)	LPE (C24:1)
24	Lyso PI (C24:0)	LPE (C29:1)
25	Lyso-PA C18:2)	LPG (C16:0)
26	Lyso-PE (R1CO2H=16:1)	LPG (C23:1)
27	Lyso-PE (R1CO2H=18:0)	LPI (C24:0)
28	Lyso-PE (R1CO2H=19:1)	LPI (C24:1)
29	Lyso-PG (C17:1)	LPI (Lyso phosphatidylinositols) (C13:1)

30	Lyso-PG (C19:0)	LPI (Lyso phosphatidylinositols) (C27:1)
31	Lyso-PG (C21:0)	LPI (Lysophospholipids) (C21:1)
32	Lyso-PG (C23:1)	Lyso PA (20:4)
33	Lyso-PG (C24:1)	Lyso-PE (R1CO2H=19:0)
34	Lyso-PG (RCO2H=15:1)	Lyso-PG (RCO2H=17:0)
35	Lyso-PG (RCO2H=18:1)	Lyso-PG (RCO2H=19:1)
36	Lyso-PG (RCO2H=19:0)	Lyso-PI (RCO2H=17:0)
37	Menaquinone MK-5 (II-H2) (C25:4)	Lyso-PI (RCO2H=18:1)
38	MG (RCO2H=14:0)	Mbt +Fe (R=17:0)
39	MG (RCO2H=15:0)	Mbt +Fe (R=17:1)
40	MG (RCO2H=16:1)	MDMB (Monodeoxymycobactins (C22:0)
41	MG (RCO2H=18:0)	MDMB (serine butyric acid monodeoxymycobactins)
42	MG (RCO2H=21:0)	MDMB(Non-ribosomal peptide/polyketide hybrids) (C19:1)
43	MG (RCO2H=22:0)	MK-6 (Menaquinones) (C30:6)
44	MPM (C30)	MMDAG (Meromycolyl diacylglycerols) (C 76:1)
45	MPM (C32)	MPM (C32)
46	MPM (C33)	PA (C29:2)
47	MPM (C34)	PA (C30:2)
48	Mycobactins (C22:1)	PA (C33:0)
49	**Mycocerosic acid (C27)**	PA (C49:2)
50	**Mycocerosic acid (C32)**	PA (Phosphatdic Acid) (C29:1)
51	**Mycolipanolic acid (C28)**	PA (Phosphatdic Acid) (C30:2)
52	**Mycosanoic or Mycocersoci acid (C26)**	PA (Phosphatdic Acid) (C32:1)
53	PA (C25)	PA (Phosphatdic Acid) (C33:1)
54	PA (C25:0)	PA (Phosphatdic Acid) (C49:2)
55	PA (C25:1)	PA (Phosphatidic Acid) (C29:1)
56	PA (C25:2)	PA (Phosphatidic Acid) (C32:1)
57	PA (C28:1)	PDIM A (C56:0)
58	PA (C29:1)	PE (25:1)
59	PA (C29:2)	PE (30:2)
60	PA (C30:2)	PE (C 34:0)
61	PA (C31)	PE (C 48:0)
62	PA (C31:2)	PE (C25:1)
63	PA (C32:1)	PE (C25:1)
64	PA (C33:1)	PE (C25:2)
65	PA (C33:2)	PE (C25:2)
66	PA (C34:1)	PE (C26:0)
67	PA (C46:1)	PE (C28:0)
68	PE (C28:1)	PE (C28:1)
69	PE (C31:0)	PE (C28:1)

70	PE (C31:1)	PE (C29:1)
71	PE (R1CO2H+R2CO2H=27:1)	PE (C30:2)
72	PE (R1CO2H+R2CO2H=28:1)	PE (C31:0)
73	PE (R1CO2H+R2CO2H=29:1)	PE (C31:1)
74	PE (R1CO2H+R2CO2H=30:0)	PE (C31:2)
75	PE (R1CO2H+R2CO2H=30:1)	PE (C32:0)
76	PE (R1CO2H+R2CO2H=31:0)	PE (C34:0)
77	PE (R1CO2H+R2CO2H=31:1)	PE (R1CO2H+R2CO2H=31:0)
78	PE (R1CO2H+R2CO2H=32:2)	PE (R1CO2H+R2CO2H=33:1)
79	PE (R1CO2H+R2CO2H=33:0)	PE (R1CO2H+R2CO2H=36:0)
80	PE (R1CO2H+R2CO2H=33:1)	PE (R1CO2H+R2CO2H=36:2)
81	PE (R1CO2H+R2CO2H=34:1)	PG (26:0)
82	PE (R1CO2H+R2CO2H=35:1)	PG (C24:2)
83	PE (R1CO2H+R2CO2H=35:2)	PG (C26:0)
84	PE (R1CO2H+R2CO2H=36:2)	PG (C26:1)
85	PE (R1CO2H+R2CO2H=39:1)	PG (C28:2)
86	PG (C24:0)	PG (C31:2)
87	PG (C24:1)	PG (R1CO2H+R2CO2H=31:2)
88	PG (C27:0)	PI (C 47:0)
89	PG (C29:1)	PI (C24:2)
90	PG (C30:2)	PI (C25:0)
91	PG (C31:2)	PI (C25:2)
92	PG (C32:2)	PI (C25:2)
93	PG (R1CO2H+R2CO2H=24:0)	PI (C33:1)
94	PG (R1CO2H+R2CO2H=24:1)	PI (R1CO2H+R2CO2H=32:2)
95	PG (R1CO2H+R2CO2H=28:0)	PI (R1CO2H+R2CO2H=33:1)
96	PG (R1CO2H+R2CO2H=28:2)	**PIM3 (R1CO2H+R2CO2H=31:0)**
97	PG (R1CO2H+R2CO2H=29:1)	**PIM4 (R1CO2H+R2CO2H=34:1)**
98	PG (R1CO2H+R2CO2H=30:2)	TAT (Triacyltrehalose)
99	PG (R1CO2H+R2CO2H=31:1)	TAT (Triacyltrehalose) (49:0)
100	PG (R1CO2H+R2CO2H=31:2)	**CL (2R1CO2H+2R2CO2H=58:2)**
101	PG (R1CO2H+R2CO2H=33:2)	**CL (2R1CO2H+2R2CO2H=59:3)**
102	PG (R1CO2H+R2CO2H=34:1)	**CL (2R1CO2H+2R2CO2H=59:3)**
103	PG (R1CO2H+R2CO2H=36:2)	PIM1 (R1CO2H+R2CO2H=34:1)
104	PG (R1CO2H+R2CO2H=37:0)	PIM2 (R1CO2H+R2CO2H=35:0)
105	PG C36:0	PIM3 (R1CO2H+R2CO2H=30:0)
106	Phosphatidic acid PA (C25:2)	PIM3 (R1CO2H+R2CO2H=33:1)
107	Phosphatidic acids (28:1)	PIM3 (R1CO2H+R2CO2H=36:0)
108	Phosphatidic acids (C32:1)	PIM6 (R1CO2H+R2CO2H=30:0)
109	**Phthioceranic acid (C36)**	
110	PI (C36:2)	
111	PI (R1CO2H+R2CO2H=32:2)	

112	PI (R1CO2H+R2CO2H=33:1)	
113	PI (R1CO2H+R2CO2H=34:1)	
114	PI (R1CO2H+R2CO2H=34:1)	
115	PI (R1CO2H+R2CO2H=36:1)	
116	PIM1 (R1CO2H+R2CO2H=37:2)	
117	**SL-II OR SL-II'(C167)**	
118	**SL-III**	
119	**TDM (C169)**	
120	TG (R1CO2H+R2CO2H+R3CO2H=73:1)	
121	**Mycolipenic acid (C27)**	
122	**Mycolipenic acid (C28)**	
123	**Mycolipenic acid (C29)**	

Table S2: List of lipids identified through LCMS in PAL fraction fractions after consulting the online mycobacterial databases.

Sr No.	PAL Fraction
1	CL (2R1CO2H+2R2CO2H=62:0)
2	DAT (C27:0)
3	Lyso-PE (R1CO2H=16:0)
4	Lyso-PE (R1CO2H=17:0)
5	Lyso-PE (R1CO2H=18:0)
6	Lyso-PE (R1CO2H=19:1)
7	Lyso-PE (R1CO2H=20:0)
8	Lyso-PG (RCO2H=16:0)
9	Lyso-PG (RCO2H=18:0)
10	Lyso-PG (RCO2H=19:1)
11	Lyso-PG (RCO2H=20:0)
12	Lyso-PI (RCO2H=18:0)
13	Lyso-PI (RCO2H=18:1)
14	Lyso-PI (RCO2H=18:1)
15	Lyso-PI (RCO2H=19:0)
16	MG (RCO2H=14:0)
17	MG (RCO2H=16:0)
18	MG (RCO2H=16:1)
19	MPM (C32)
20	Mycolipanolic acid (C27)
21	PE (R1CO2H+R2CO2H=31:0)
22	PE (R1CO2H+R2CO2H=33:1)
23	PE (R1CO2H+R2CO2H=36:0)
24	PE (R1CO2H+R2CO2H=36:2)
25	PG (R1CO2H+R2CO2H=30:2)
26	PG (R1CO2H+R2CO2H=31:0)

27	PG (R1CO2H+R2CO2H=31:2)
28	PG (R1CO2H+R2CO2H=37:0)
29	PG (R1CO2H+R2CO2H=30:2)
30	PG (R1CO2H+R2CO2H=36:2)
31	PG (R1CO2H+R2CO2H=37:0)
32	PI (R1CO2H+R2CO2H=33:2)
33	PI (R1CO2H+R2CO2H=34:1)
34	PI (R1CO2H+R2CO2H=37:1)
35	PI (R1CO2H+R2CO2H=42:1)
36	PIM1 (R1CO2H+R2CO2H=32:1)
37	PIM1 (R1CO2H+R2CO2H=37:0)
38	Hydroxyphthioceranic acid (C39)
39	Hydroxyphthioceranic acid (C40)
17	Mycocerosic acid (C30)
18	Mycocerosic acid (C32)
19	Mycocerosic acid (C35)
20	DG (R1CO2H+R2CO2H=33:0)
21	DAG (R1CO2H+R2CO2H=34:2)
22	Mycolipanolic acid (C26)
23	Mycolipenic acid (C27)
24	Mycolipenic acid (C28)
25	Mycolipenic acid (C29)
26	Mycosanoic or Mycocerosic acid (C24)
30	Phthioceranic acid (C36)
31	Phthioceranic acid (C45)

SI Materials

KEY RESOURCES TABLE

REAGENT or RESOURCE	SOURCE	IDENTIFIER
Antibodies		
Monoclonal Anti-Mycobacterium smegmatis LAM	BEI resources	Cat # NR-13798
Pierce Goat Anti-Mouse HRP conjugate	ThermoScientific	Cat # 31430
Fluorophores		
16:0 LissRhod PE	Avanti Polar Lipids	Cat # 810158
TopFluor Cholesterol	Avanti Polar lipids	Cat # 810255
1,6-Diphenyl-1,3,5-hexatriene	Sigma-Aldrich	Cat # D208000
6-dodecanoyl-N,N-dimethyl-2-napthalmine	Sigma-Aldrich	Cat # 40227
TMA-DPH	Cayman Chemical Company	Cat # 17294
Bacterial and Virus Strains		
Mycobacterium smegmatis mc^2155	Prof. Roop Lal (Delhi University)	Generous gift
Chemicals, Peptides, and Recombinant Proteins		
Middlebrook 7H9 Broth Base	HiMedia	Cat # M198
Bovine Serum Albumin	HiMedia	Cat # MB083
α-D-Glucose	SIGMA-ALDRICH	Cat # 158968
Catalase from bovine liver	SIGMA-ALDRICH	Cat # C9322
Glycerol Anhydrous	EMPARTA	Cat # 1.07051.0521
Dioctyl Sulfosuccinate Sodium Salt	SIGMA-ALDRICH	Cat # 323586
n-Heptane	EMPARTA	Cat # 1.07053.0521
Chloroform	EMAPRTA	Cat # 1.07024.2521
Chloroform (For UV Spectroscopy)	Spectrochem	Cat # 050304
Lysozyme	HiMedia	Cat # MB098
Phosphomolybdic Acid	Loba Chemie	Cat # 51429-74-4
Anthrone	Sigma-Aldrich	Cat # 319899
Deuterium oxide	Sigma-Aldrich	Cat # 151882
Trizma base	Sigma-Aldrich	Cat # T1503
Magnesium chloride hexahydrate	Sigma-Aldrich	Cat # M2393
Magnesium Chloride anhydrous	Spectrochem Pvt. Ltd.	Cat # 0113205
Sulphuric Acid	EMPARTA	Cat # 1.93000.0521
Tween 80	Merck	Cat # 8.22187.0521
N,N'-Methylenebisacrylamide	Sigma-Aldrich	Cat # M7279
Acrylamide	HiMedia	Cat # MB068

N,N,N',N'-Tetramethylethylenediamine	Sigma-Aldrich	Cat # T9281
Ammonium persulfate	Sigma-Aldrich	Cat # A3678
Glycine	EMPARTA	Cat # 1.94907.0521
Tetrabutylammonium Hydroxide	Spectrochem Pvt. Ltd.	Cat # 0120274
Methyl Iodide	Spectrochem Pvt. Ltd.	Cat # 011361
Acetonitrile For Chromoatography	EMPARTA	Cat # 61803025001730
Methanol Spectroscopic grade	Sigma-Aldrich	Cat # 154903
Ethanol absolute	CSS	
Sodium dodecyl sulfate	EMPLURA	Cat # 1.94954.0521
Bromophenol Blue	HiMedia	Cat # MB123
Phenol	EMPARTA	Cat # 1.94903.0521
Petroleum Ether	Detec	Cat # V800297
Dichloromethane	MembaChem Industried Pvt.Ltd.	Cat # 300126
1, 2 –dioleoyl-sn-glycero-3-phosphocholine (DOPC)	Avanti Polar Lipids	Cat # 850375P
1, 2 dipalmitoyl –sn-glycero-3 phospho- (1'-rac-glycerol) sodium salt (DPPG)	Avanti Polar Lipids	Cat # 840455
Phosphate buffer Saline	HiMedia	Cat # RM7385
Diethyl ether	RANKEM	Cat # D2320
Hydrochloric acid	EMPARTA	Cat # 1.93001.0521
Tricine	Sigma Aldrich	Cat # T0377
Mycolic acids	Sigma Aldrich	Cat # M4537
Software and Algorithms		
IgorPro 6.37	Wavemetrics	Cat # Igor Pro (Freeware)
Asylum Research version 14.30.157	Asylum Research	Freeware
Zen Lite 2.3	Carl Zeiss	Freeware
GRAMS/AI™ Spectroscopy Software	Thermo Scientific	Cat # INF-15000
GraphPad Prism	GraphPad Ver. 5.0	
Other		
TLC silica gel 60 F_{254}	Merck	Cat # 1.05554.007
Silica gel 100-200 mesh	Finar	Cat # 11448S5K25
ITO coated cover slips	SPI Supplies	Cat # 06486-AB
PELCO Mica Discs 9.9mm Diamter	Ted Pella, Inc	Cat # 50
AFM Probe	Asylum Research	Cat # BL-TR400PB
Cell Culture Dish 60mm*15mm	Genaxy	Cat # GEN-PTD-60
C18 LCMS column	Thermoscientific	Cat # 25003-102130